Oil & Natural Gas Technology

DOE Award No.: DE-FE0010406
DUNS No.: 170230239

Quarterly Research Performance Progress Report
(Period ending 12/31/2014)

CONTROLS ON METHANE EXPULSION DURING MELTING OF NATURAL GAS HYDRATE SYSTEMS: TOPIC AREA 2
Project Period (9/30/2013 to 9/30/2015)

Submitted by:
Peter B. Flemings

_____
Signature

The University of Texas at Austin
101 East 27th Street, Suite 4.300
Austin, TX 78712-1500
e-mail: pflemings@jsg.utexas.edu
Phone number: 512-475-9520

Prepared for:
United States Department of Energy
National Energy Technology Laboratory

January 30, 2015

Office of Fossil Energy

1 ACCOMPLISHMENTS:

1.1 *What are the major goals of the project?*

The project goal is to predict, given characteristic climate-induced temperature change scenarios, the conditions under which gas will be expelled from existing accumulations of gas hydrate into the shallow ocean or directly to the atmosphere. When those conditions are met, the fraction of the gas accumulation that escapes and the rate of escape shall be quantified. The predictions shall be applicable in Arctic regions and in gas hydrate systems at the up dip limit of the stability zone on continental margins. The behavior shall be explored in response to two warming scenarios: longer term change due to sea level rise (e.g. 20 thousand years) and shorter term due to atmospheric warming by anthropogenic forcing (decadal time scale).

	Milestone Description	Planned Completion	Actual Completion	Comments (progress toward achieving milestone, explanation of deviation from plan, etc.)
Phase 1	**1.A** 1-D simulation of gas hydrate dissociation in natural systems.	9/30/2013	9/30/2013	Complete
	1.B 1-D Simulation of gas hydrate dissociation in laboratory controlled conditions.	3/31/2014	11/1/2013	Complete
	1.C Model-based determination of conditions required for gas not to reach seafloor/atmosphere from dissociating hydrate accumulation.	3/31/2014	3/31/2014	Complete
	1.D Determination of what hydrate reservoirs are at three-phase equilibrium.	12/31/2013	12/1/2013	Complete
	1.E Demonstrate ability to create and dissociate methane hydrate within sediment columns under conditions analogous to natural systems.	9/30/2013	10/15/2013	Complete
Phase 2	**2.A** 1-D simulation of gas expulsion into hydrate stability zone.	9/29/2014	9/29/2014	Complete
	2.B Determination of conditions for which gas expulsion into hydrate-stability zone is self-limiting.	12/29/2014	9/29/2014	Complete
	2.C Demonstration of reaction transport experiment where gas invades hydrate stability zone and creates three phase stability.	9/30/2015		Currently developing/refining remote sensing technologies. Refining experimental design based on numerical simulation
	2.D Demonstrate a 2D simulation of hydrate dissociation and gas expulsion.	3/31/2015		Currently developing these simulations

1.2   What was accomplished under these goals?

PHASE 1/BUDGET PERIOD 1

Task	Projected Finish	Actual Finish	Summary
Task 1: Project Management and Planning	9/30/15	In process	Monitoring & controlling project
Task 2: Conceptual and Numerical Model Development -1D	3/31/14	3/31/14	Task 2 has been completed.
Task 3: Categorize stability of known hydrate reservoirs	9/30/13	9/30/13	Task 3 has been completed.
Task 4: Laboratory Evaluation of Hydrate Dissociation	3/31/14	6/1/14	Task 4 has been completed.

PHASE 2/BUDGET PERIOD 2

Task 5: Gas expulsion modeling
Projected Finish: 9/28/15
Actual Finish: in process

Subtask 5.1 - Develop 1D model of gas expulsion into water-saturated hydrate-stability zone
Projected Finish: 9/29/14
Actual Finish: 9/29/14
We have fully developed a 1D numerical model. Results have been presented in previous quarterly reports (June & October 2014). Our work has led us to explore two additional models arguments: 1) An analytical approach to the 1D modeling and 2) A numerical approach to look at hydrate in fractures.

We develop an analytical model using method of characteristics to describe the one-dimensional hydrate system development in this section. Fig. 1 is a schematic diagram of the model. The sediment is initially fully saturated with brine of salinity cl_0. The sediment has a uniform temperature T_0 and a small pressure gradient with an average pressure of P_0. The initial system is in hydrate stability zone. Methane gas is injected with a fixed rate of q_{gi} and density of ρ_{gi} from the left end. Methane hydrate forms from the gas inlet and increases the local salinity to three-phase equilibrium value, when no more hydrate can form. Hydrate solidification front and gas front moves further into the sediment (rightward). We neglect the hydrate formation kinetics because hydrate formation is rapid as shown by laboratory (Zatsepina and Buffett, 2003) and field (Rehder et al., 2002) studies. Therefore, gas saturation is zero at the downstream side of the hydrate solidification front (point *a* in Fig. 1). It increases gradually from the hydrate solidification front to the gas inlet (Fig. 1). We also neglect the diffusion transport.

This semi-infinite system contains three phases (subscript κ), gas (g), liquid water (l) and hydrate (h) phases, and three components (subscript β), brine with the three-phase equilibrium salinity (B), pure water (W) and methane (M).

The mass conservation equation for methane is

$$\frac{\partial G_M}{\partial \tau} + \frac{\partial H_M}{\partial \varepsilon} = 0, \tag{1}$$

where τ is the dimensionless time; ε is the dimensionless distance from the gas inlet; G_M is the dimensionless overall concentration of methane; and H_M is the dimensionless overall flux of methane. These parameters are defined as

$$\tau = \frac{q_{gi}t}{L\phi}, \tag{2}$$

$$\varepsilon = \frac{x}{L}, \tag{3}$$

$$G_M = X_{M,l}\rho_{lD}S_l + X_{M,g}\rho_{gD}S_g + X_{M,h}\rho_{hD}S_h, \tag{4}$$

$$H_M = v_D\left(X_{M,l}\rho_{lD}f_l + X_{M,g}\rho_{gD}f_g\right), \tag{5}$$

where t is time (sec); L is characteristic length (m); ϕ is porosity of the sediment (m³ m⁻³); $X_{M,l}$, $X_{M,g}$ and $X_{M,h}$ are the mass fraction of methane (dimensionless) in liquid water, gas and hydrate phases, respectively; ρ_{lD}, ρ_{gD} and ρ_{hD} are the dimensionless density of liquid water, gas and hydrate phases, respectively, and $\rho_{lD} = \dfrac{\rho_l}{\rho_{gi}}$, $\rho_{gD} = \dfrac{\rho_g}{\rho_{gi}}$, $\rho_{hD} = \dfrac{\rho_h}{\rho_{gi}}$; ρ_l, ρ_g and ρ_h are the density of liquid water, gas and hydrate phases (kg m⁻³), respectively; S_l, S_g and S_h are the saturation of liquid water, gas and hydrate phases (dimensionless), respectively; v_D is the dimensionless total flux, and $v_D = {v}/{q_{gi}}$; v is the total flux (m sec⁻¹) of the mobile phases; f_l and f_g are the fractional flow of liquid water and gas phases (dimensionless), respectively.

$$f_g = \frac{\lambda_g}{\lambda_g + \lambda_l}\left[1 + \frac{k\lambda_l}{v}\left(\frac{\partial P_c}{\partial x} + (\rho_l - \rho_g)g\sin\theta\right)\right], \tag{6}$$

$$f_l = 1 - f_g, \tag{7}$$

where λ_l and λ_g are the mobility (Pa⁻¹ sec⁻¹) of gas and liquid water phases, respectively, and $\lambda_g = {k_{rg}}/{\mu_g}$, $\lambda_l = {k_{rl}}/{\mu_l}$; k_{rg} and k_{rl} are the gas and liquid water phase relative permeabilities (dimensionless), respectively; μ_g and μ_l are the gas and water dynamic viscosities (Pa sec), respectively; k is the intrinsic permeability of the sediment (m²); g is the gravitational acceleration (m sec⁻²); θ is the dip angle measured as the angle between the flow direction and a horizontal line (rad); P_c is the capillary pressure between the gas and liquid water phases (Pa). f_g can be broken into three

components: a viscous component ($\frac{\lambda_g}{\lambda_g + \lambda_l}$), a capillary component ($\frac{\lambda_g}{\lambda_g + \lambda_l} \frac{k\lambda_l}{v} \frac{\partial P_c}{\partial S_g} \frac{\partial S_g}{\partial x}$) and a

gravity component ($\frac{\lambda_g}{\lambda_g + \lambda_l} \frac{k\lambda_l}{v} (\rho_l - \rho_g) g \sin\theta$) (DiCarlo et al., 2012).

According to method of characteristics (Orr, 2007), the overall concentration of methane G_M does not change with time on the characteristic curve

$$\xi = \frac{\partial H_M}{\partial G_M} \tau + \varepsilon_0 , \tag{8}$$

where ε_0 is the initial dimensionless position of the composition G_M. The same procedure can be applied to the component of pure water and brine with three-phase equilibrium salinity.

A leading shock develops at the hydrate solidification front where the system changes from three phases to one phase (Orr, 2007) (Fig. 1). The shock wave velocity equals the composition wave velocity at b in Fig. 1. Each component must have the same shock wave velocity. Therefore,

$$\Lambda_B^{ab} = \Lambda_W^{ab} , \tag{9}$$

$$\Lambda_B^{ab} = \Lambda_M^{ab} , \tag{10}$$

$$\Lambda_B^{ab} = \frac{\partial H_\beta}{\partial G_\beta} |_b = v_D^b \frac{\partial f_g}{\partial S_g} |_{S_g = S_g^b} , \tag{11}$$

where the superscripts a and b means the downstream and upstream side of the leading shock, respectively; Λ_β^{ab} is the dimensionless leading shock velocity calculated by the component β. It is also the dimensionless hydrate solidification front advancing velocity and is expressed as

$$\Lambda_\beta^{ab} = \frac{H_\beta^a - H_\beta^b}{G_\beta^a - G_\beta^b}, \quad \beta = B, W, M . \tag{12}$$

If the capillary component of the gas fractional flow f_g is neglected, we can obtain the hydrate (S_h), liquid water (S_l) and gas phase saturations (S_g) at b and the ratio of the flux between a and b (v_D^a / v_D^b) by solving the nonlinear equation group of Eqs. (6), (7) and (9)-(12). The trailing shock calculation provides the saturations at point c in Fig. 1.

The total liquid water and gas phase flux between c and b is uniform and equals that at c or b because it is in the three-phase region and the phase compositions are fixed (Orr, 2007). Therefore, composition wave velocity between c and b can be calculated as (Orr, 2007)

$$\Lambda^e = v_D^c \frac{\partial f_g}{\partial S_g} |_{S_g = S_g^e} , \tag{13}$$

where S_g^e is an arbitrary gas saturation between c and b or between S_g^c and S_g^b; Λ^e is the dimensionless composition wave velocity for gas saturation of S_g^e. At the dimensionless time τ, the dimensionless distance between the place where gas saturation equals S_g^e and the gas inlet ξ^e is calculated as

$$\xi^e = \Lambda^e \tau .$$
(14)

Hydrate saturation is homogeneous from *c* to *b* ($S_g^c = S_g^b$). That is because the system initial condition is nearly homogeneous and we neglect the salt diffusion. Hydrate and liquid water phase saturation at ξ^e (S_l^e) are

$$S_h^e = S_h^b ,$$
(15)

$$S_l^e = 1 - S_g^e - S_h^e .$$
(16)

Fig. 2 shows the characteristics of an example calculation with the parameters listed in Table 1. The saturations of each phase does not change along the characteristics (Fig. 2). The characteristics for the initial composition (100% liquid water) emanate from $\tau = 0$ and have the slope of 5.9 (red lines in Fig. 2). The characteristics for the injection composition (100% gas) emanates from $\tau = 0$ and along the $\xi = 0$ line (Fig. 2). There is a trailing shock from the injection composition to the gas saturation of 28.5%, but it has zero wave velocity. Therefore, the fan of characteristics for the discontinuity initially present at the gas inlet extends all the way from the gas saturation of 10.7% to $\xi = 0$. Leading shock happens where the characteristic of gas saturation 10.7% intersects the initial composition (red lines in Fig. 2). Any line in the characteristics figure that is parallel to the line of $\tau = 0$ provides the saturation distribution along the column at a certain time. Any line that is parallel to the line of $\xi = 0$ provides the system composition evolution with time at a certain distance from the gas inlet (Fig. 3).

The hydrate solidification front advancing velocity or the leading shock wave velocity is 0.63 cm hour[-1]. The hydrate saturation is 68.4% behind the hydrate solidification front (Fig. 3). The gas saturation continuously decreases from 28.5% (point *c*) to 10.7% (point *b*), and water saturation continuously increases from 3.1% (point *c*) to 20.9% (point *b*) (Fig. 3). Hydrate formation at the hydrate solidification front causes total volume loss and decreases the total flux from 10^{-6} m sec^{-1} (point *b*, *c* and *d*) to 1.71×10^{-7} m sec^{-1} (point *a*).

Liu and Flemings (2007) developed a fully coupled multiphase multicomponent fluid flow and mass transport numerical model to simulate the methane hydrate formation and dissociation dynamics. We did two simulations to investigate the hydrate system development using this model with the same parameters listed in Table 1. The first one considers the capillary pressure (dashed lines in Fig. 3), and the second one neglects the capillary pressure (dotted lines in Fig. 3). Compared with these two numerical simulations, the hydrate saturation calculated by the analytical solution are lower while the gas saturation are higher (Fig. 3). Hydrate solidification front calculated by the analytical solution moves a little faster than the numerical simulations (Fig. 3). The analytical solution matches much better with the numerical simulation neglecting the capillary pressure effect (solid lines are more close to the dotted lines than to the dashed lines), because we did not include the capillary component in the fractional flow curve in this analytical simulation. The difference between the analytical and numerical results neglecting the capillary pressure close to the gas inlet is caused by the boundary effect in the numerical simulation. Their difference at the leading shock is caused by the fact that the numerical solution inevitably has numerical diffusion causing smearing of shocks.
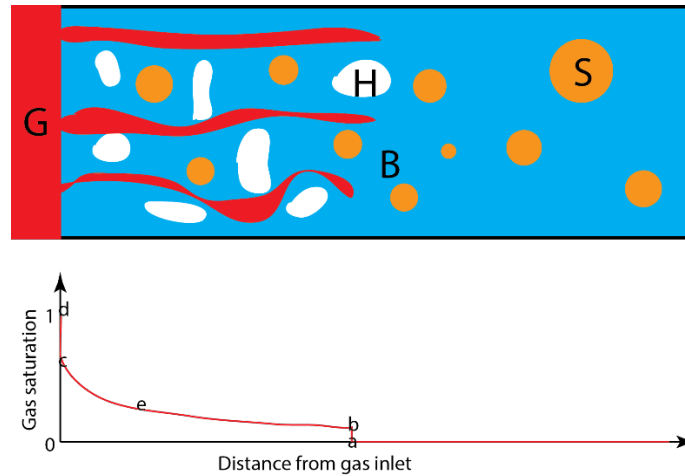
Figure 1: Schematic diagram of methane gas injection into a brine saturation sediment within methane hydrate stability zone. The system reaches three-phase equilibrium behind the hydrate solidification front, and brine with an increased salinity coexists with methane gas and hydrate. The red line in the lower figure shows the schematic of gas saturation distribution. Gas saturation decreases from 100% at the upstream side of the gas inlet (point d in the lower figure) to 0% at the downstream side of hydrate solidification front (point a in the lower figure). G means methane gas, H means hydrate, B means brine and S means solid grain. a and b means downstream and upstream side of the leading shock, respectively. c and d means downstream and upstream side of the trailing shock, respectively. e means the position where the gas saturation equals an arbitrary value S_g^e **between that of the trailing and leading shocks.**
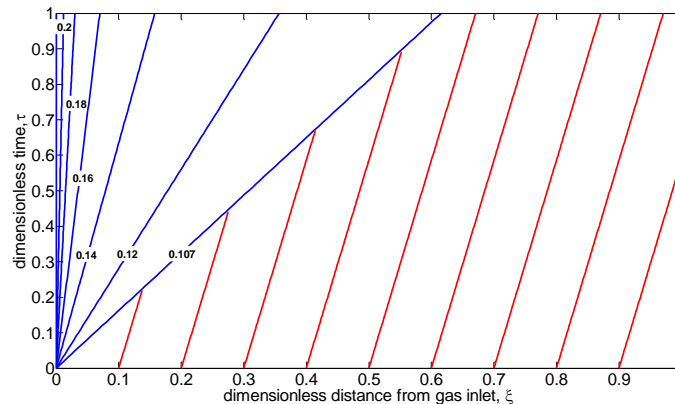

Figure 2: Characteristics for methane gas injection into a horizontally-placed brine-saturated sediment with pressure of 6.89 MPa, temperature of 4 °C, initial salinity of 3 wt.% and gas injection rate of 10^{-6} **m sec⁻¹. The blue lines are the characteristics for the discontinuity initially present at the gas inlet. Numbers on the blue lines are gas saturations. The red lines are the characteristics for the initial composition in the sediment, where the gas saturations are zero. The line** $\tau = 0$ **is the characteristics for the injection composition.**
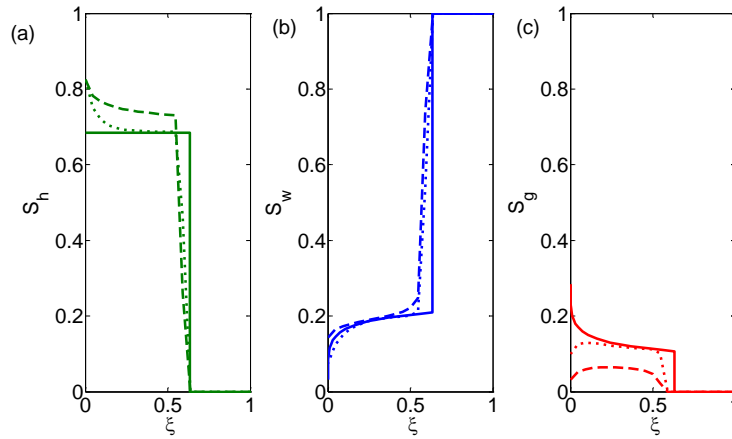
Figure 3: Hydrate (S_h, green lines, Fig. 4a), water (S_w, blue lines, Fig. 4b) and gas (S_g, red lines, Fig. 4c) saturation distributions in the sediment at dimensionless time 1.0 calculated by the analytical solution (solid lines), the numerical solution developed in Liu and Flemings (2007) with capillary pressure (dashed lines) and the numerical solution without capillary pressure (dotted lines).

Table 1: Parameters used in the example calculation.

Viables	Physical meanings	Values
P_0	Pressure (MPa)	6.89
T_0	Temperature (^oC)	4
cl_0	Initial salinity (wt.%)	3
cl_e	Three-phase equilibrium salinity (wt.%)	10.96
L	Column length (m)	0.11
q_{gi}	Methane gas injection rate (m sec^{-1})	10^{-6}
ρ_{gi}	Density of gas injected (kg m^{-3})	56
ϕ	Porosity in absence of hydrate	0.35
ρ_h	Hydrate density (kg m^{-3})	912
k_0	Sediment intrinsic permeability without hydrate (m^2)	10^{-13}
θ	Dip angle of the system (rad)	0
S_{gr}	Residual gas saturation	0.02
S_{wr}	Residual water saturation	0.1
μ_g	Gas dynamic viscosity (Pa sec)	2×10^{-5}
μ_l	Liquid water phase dynamic viscosity (Pa sec)	1.31×10^{-3}
$X_{M,h}$	Mass fraction of methane in hydrate (wt.%)	13.4
$X_{W,h}$	Mass fraction of water in hydrate (wt.%)	86.6

Over the last quarter, we have been looking further into the hypothesis that narrow, hydrate-filled fracture networks act as conduits for vertical gas migration through the hydrate stability zone. Our previous petrophysical analysis of various hydrate-bearing sites, supported by additional published studies, has revealed that, in fine-grained material, hydrate frequently forms in high-angle fractures (Daigle et al., 2011; NGHP Expedition 01 Scientists, 2007; Rees et al., 2011; Riedel et al., 2010; Ryu et al., 2013). It is commonly hypothesized that these fractures form from the development of a gas reservoir beneath the GHSZ with a pore pressure that overcomes the least principle stress and creates hydraulic fractures in the overlying sediment (Daigle et al., 2011; Daigle and Dugan, 2011). Seafloor methane gas vents are also frequently observed above hydrate-filled fracture networks (Bangs et al., 2011; Haeckel et al., 2004; Torres et al., 2011), which suggests that these fracture networks also act as conduits for gas migration (Daigle et al., 2011; Haacke et al., 2009; Mazumdar et al., 2009).

This observation has led researchers to question the mechanism that allows the vertical migration of gas in these fractures through the hydrate stability zone. Three primary hypotheses have been proposed (Figure 4). First, the kinetics of hydrate formation limit hydrate precipitation such that gas can migrate through the fractures without forming hydrate (Haeckel et al., 2004; Torres et al., 2004). Second, hydrate formation is limited by the amount of water available in the fracture such that, after some initial hydrate formation and gas consumption, hydrate ceases to precipitate and gas can migrate vertically (Clennell et al., 1999; Ginsburg and Soloviev, 1997). Finally, hydrate formation elevates the salinity in the pore water, producing three-phase equilibrium conditions and limiting the formation of additional hydrate, which allows the gas to pass through the remaining pore space (Liu and Flemings, 2006; Meyer and Flemings, 2014; Milkov et al., 2004). As we have moved forward in our research concerning the formation of hydrate in fractures, we focused on this final hypothesis as the primary mechanism for vertical gas migration, assuming that formation kinetics are negligible and that there is always water available to form hydrate.
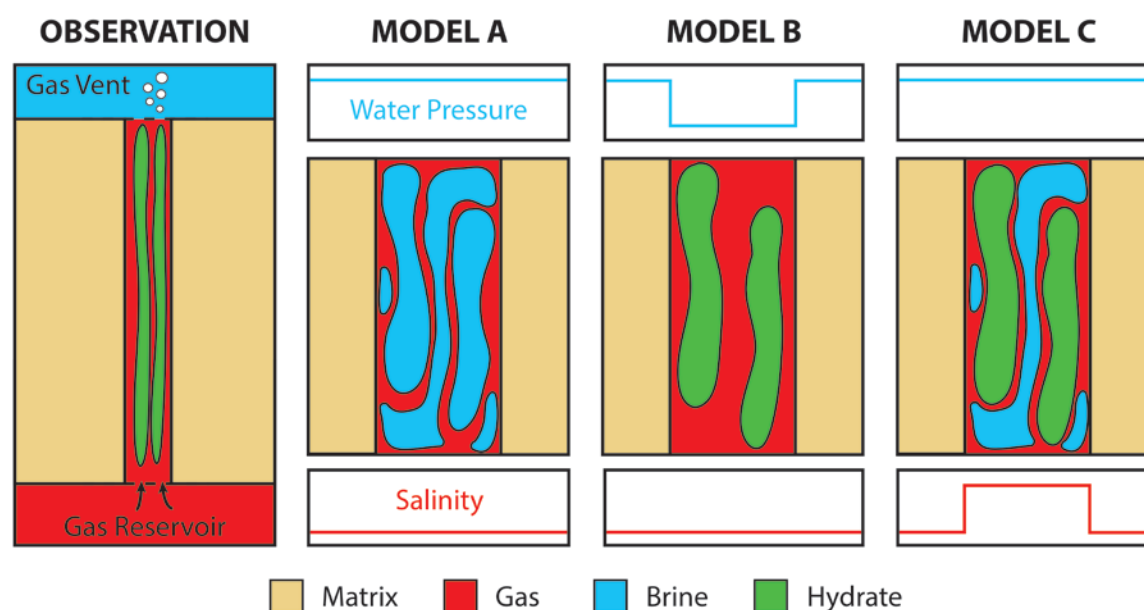

Figure 4: Cartoon describing the three major hypotheses presented to explain the observed methane gas vents associated with hydrate-filled fractures. Model A indicates that hydrate formation is limited by kinetics. Model B states that the hydrate consumes the readily available water and becomes water limited. Model C suggests that hydrate formation can locally elevate salinity and restrict hydrate formation.

To gain some initial understanding of the physics controlling this process, we have developed a numerical model describing the movement of water and salt associated with the formation of hydrate in fractures. We are specifically interested in osmotic pressure as a potential driving force for fluid flow. The intrinsic osmotic pressure of a fluid is calculated with Equation 17 (Malusis et al., 2003):

$$u_{os} = -\omega \cdot v \cdot R \cdot T \cdot C \tag{17}$$

where ω, v, R, T, and C are the chemico-osmotic efficiency coefficient, ion reaction constant, gas constant (8.314 J/mol-K), temperature (K), and salt concentration, respectively. The ω-value describes how ideally semi-permeable a membrane acts. A value of $\omega = 1$ indicates an ideally semi-permeable membrane, while $\omega = 0$ indicates a fully permeable membrane. A membrane with a $\omega > 0$ separating two fluids of different salinities, will produce an osmotic pressure gradient that can result in fluid flow (Bader and Kooi, 2005). In our model, we assume a matrix of fine-grained material, which has been shown to act as a non-ideal, semi-permeable membrane. Although the ω-value is dependent on the porosity of the material and salt concentration of the fluid, it is typically non-zero (Barbour and Fredlund, 1989).
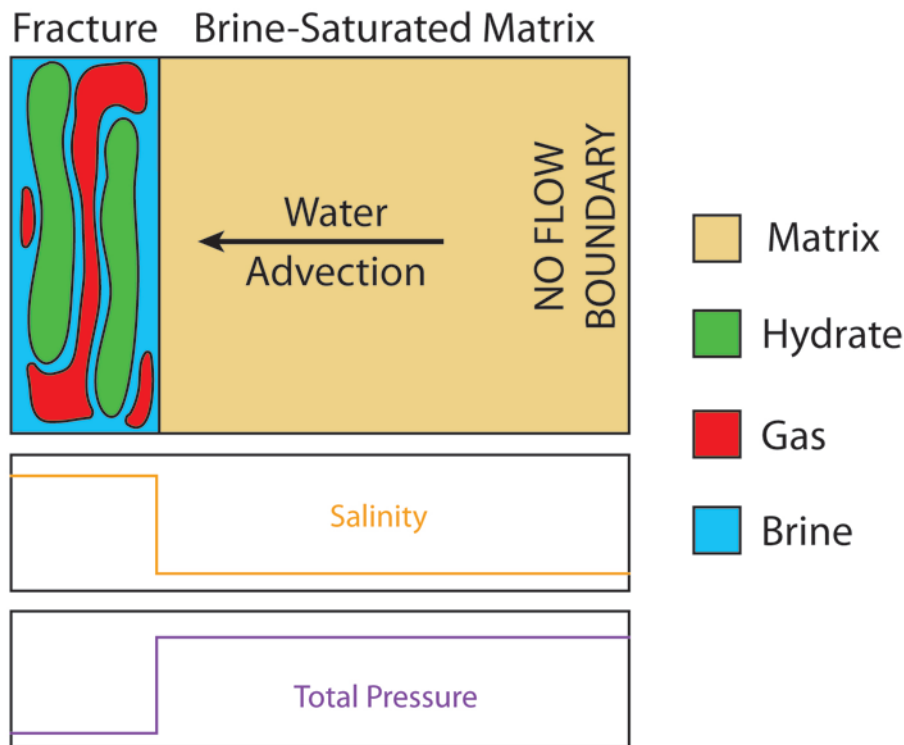

Figure 5: General conceptual model of osmotic pressure as a potential mechanism for water flow toward a fracture to support hydrate formation. Elevated salinity in the fracture, due to hydrate formation, reduces the total pressure in the fracture. This produces a pressure gradient that induces water advection toward the fracture.

The model domain extends from the fracture wall to the half-fracture spacing and the model keeps track of the fluid overpressures (total, water, and osmotic), salinity, and porosity within the domain over time (Figure 5). External to the domain, within the fracture, the formation of hydrate increases the salinity of the water proximal to the fracture wall, increasing the osmotic pressure and decreasing the total pressure relative to hydrostatic pressure within the domain. This pressure gradient produces a driving

force for the advection of water and salt from the matrix into the fracture, which supports the continual hydrate formation and salinity elevation. The model holds the following assumptions:

a. One-dimensional model (homogeneous material)
b. Constant water density
c. Darcy's Law applied for water flow
d. No salt diffusion
e. Matrix acts a non-ideal semi-permeable membrane (ω = 0.01)
f. All the water that enters the fracture forms hydrate
g. Hydrate formation kinetics are negligible

Using water and salt mass balance and Darcy's Law, we derived the follow water (Eq. 18) and salt (Eq. 19) advection equations and half-fracture thickness (Eq. 20) calculation:

$$\frac{du_w}{dt} = \left[\frac{k \cdot (1+e)^2 \cdot \sigma' \cdot \ln(10)}{C_c \cdot \mu} \right] \cdot \frac{du_{tot}}{dx} \tag{18}$$

$$\frac{d(\phi C)}{dt} = -\frac{d(q_w C)}{dx} \tag{19}$$

$$q_w = -\frac{k}{\mu} \frac{\partial (u_w - u_{os})}{\partial x} \tag{20}$$

$$L_{frac} = \left[\frac{\rho_w}{\left(\rho_h \cdot \left(\frac{M_w}{M_H} \cdot n \right) \right)} \right] \cdot \int_0^t q_w (x = 0)_t \cdot dt \tag{21}$$

We then discretized equations B and C and solved them using an explicit, numerical method. The values for permeability (k) and compression index (C_c) were estimated from geotechnical tests previously performed on Resedimented Boston Blue Clay (RBBC) material (Schneider, 2011). The model was run on a domain 2 meters wide over a period of 1 year in order to achieve pressure equilibrium.

The model results (Figures 6) express the following initial and boundary conditions as the solid lines:

a. Constant hydrostatic pressure and three-phase salinity at fracture boundary
b. No flow boundary at the half-fracture spacing
c. Initially seawater salinity and hydrostatic pressure throughout the domain

Once the model starts, water flows down the pressure gradient toward the fracture, decreasing the water and total pressure in unison (Figure 6a). The reduction in water pressure results in a decrease in effective stress and a 0.33 percent decrease in porosity due to consolidation (Figure 6b). Additionally, the consolidation resulted in a 0.33 percent increase in salinity (Figure 6c). After a year, the total pressure reaches equilibrium across the domain and water ceases to flow into the fracture (Figure 6d). At this point, the amount of water that entered the fracture would make a hydrate-filled fracture approximately 1.6cm thick (Figure 6e).

This model is a relatively simplistic look at the physics controlling hydrate formation in fractures; however the results provide some interesting initial understanding into this problem. The model uses well supported fluid flow physics with constrained sediment characteristics and produced a fracture thickness that is reasonable compared to those found in nature. This suggests that osmotic pressure gradients across fracture boundaries could be a reasonable driving force for water flow into a fracture and continual hydrate formation. From this point, we will be continuing our research in this area with additional model advancements, including salt diffusion, capillary-induced flow, and cryogenic suction effects.
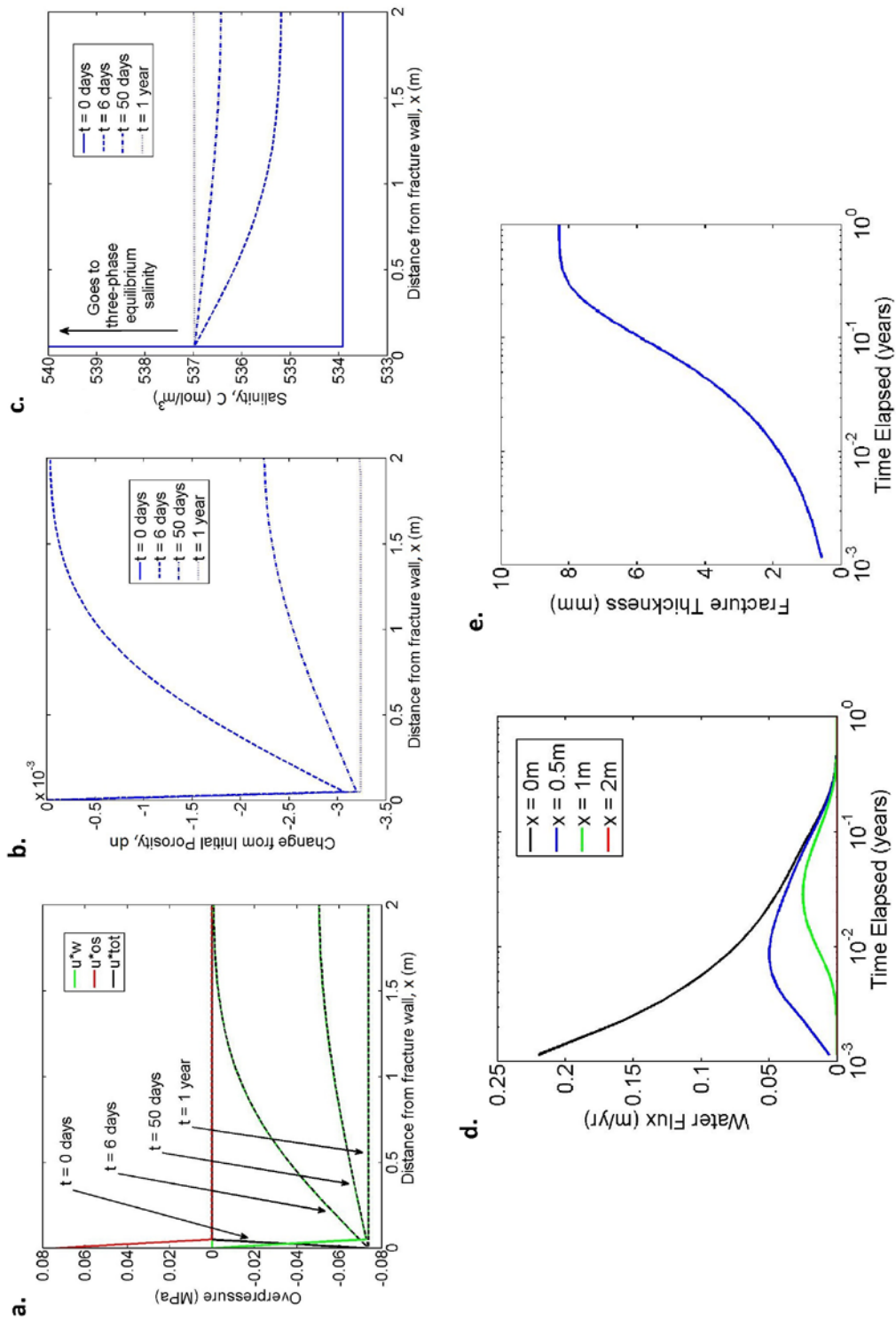
Figure 6: Compilation of the 1-year advection model results. A) Total (u*tot), water (u*w), and osmotic (u*os) overpressure profiles throughout time. B) Porosity profile across the domain during the model. C) Salt concentration within the matrix throughout time. D) Water flux over time at various points within the matrix. E) Fracture half-thickness as a function of time. Over the course of the model, water flows out of the matrix and into the fracture, reducing overpressures, porosity, and water flux and increasing salinity and fracture half-thickness.

Subtask 5.2 - Apply 1D expulsion to laboratory experiments

Projected Finish: 3/30/15
Actual Finish: 9/29/14
The model has been developed and presented in the June 2014 report.

Subtask 5.3 - Apply 1D model to natural hydrate accumulations

Projected Finish: 9/28/15
Actual Finish: in process
The model is currently being applied to the permafrost zone and to the deepwater continental margins.
Presented in the October 2014 report

Task 6: Gas expulsion experiments

Projected Finish: 9/28/15
Actual Finish: in process

Subtask 6.1 - Gas invasion into water-saturated hydrate saturated zone

Projected Finish: 12/29/14
Actual Finish: in process

As reported in our previous Quarterly Report (Sept 2014), we have not yet successfully modeled gas invasion into the hydrate stability field. In our previous attempt, we could not get a clear gas invasion front. Over the last quarter, we:

- Refurbishing LBNL pressure cell and reassembling
- Completed drainage tests
- Limited participation in design of UT hydrate cell
- Team meeting at the American Geophysical Union Fall Meeting in San Francisco in December

The LBNL hydrate pressure cell required refurbishing due to small corrosion pits on the outside. These pits were noticed as part of routine inspections required as part of the safety requirements. The cylinder was replaced, and the cooling jacket design modified to include a Teflon layer between the coolant and the aluminum vessel.

The drainage tests reported in the last quarter were completed and analysis completed. No changes to our conclusions were required.

Several opportunities for feedback of the UT hydrate system resembling the LBNL system arose, resulting in limited design collaboration.

Team members attending the American Geophysical Union Fall Meeting in San Francisco in December met for several discussions on project accomplishments and direction. These discussions resulted in resolving some experimental unknowns, and further analysis of both UT and LBNL experimental equipment designs.

In combination with our progress at the Lawrence Berkeley National Laboratory, we have continued our efforts to begin experimentation at the University of Texas at Austin. As reported in our previous Quarterly Report, we have purchased all the materials necessary to begin experiments and have built the aluminum hydrate formation pressure vessel and cooling jacket. Over the past quarter, we constructed the vessel hanger and assembled the fittings, tubing, plumbing, valves, and rupture disc, and put the whole system together (Figures 7 and 8) to determine any additional materials that might be missing.
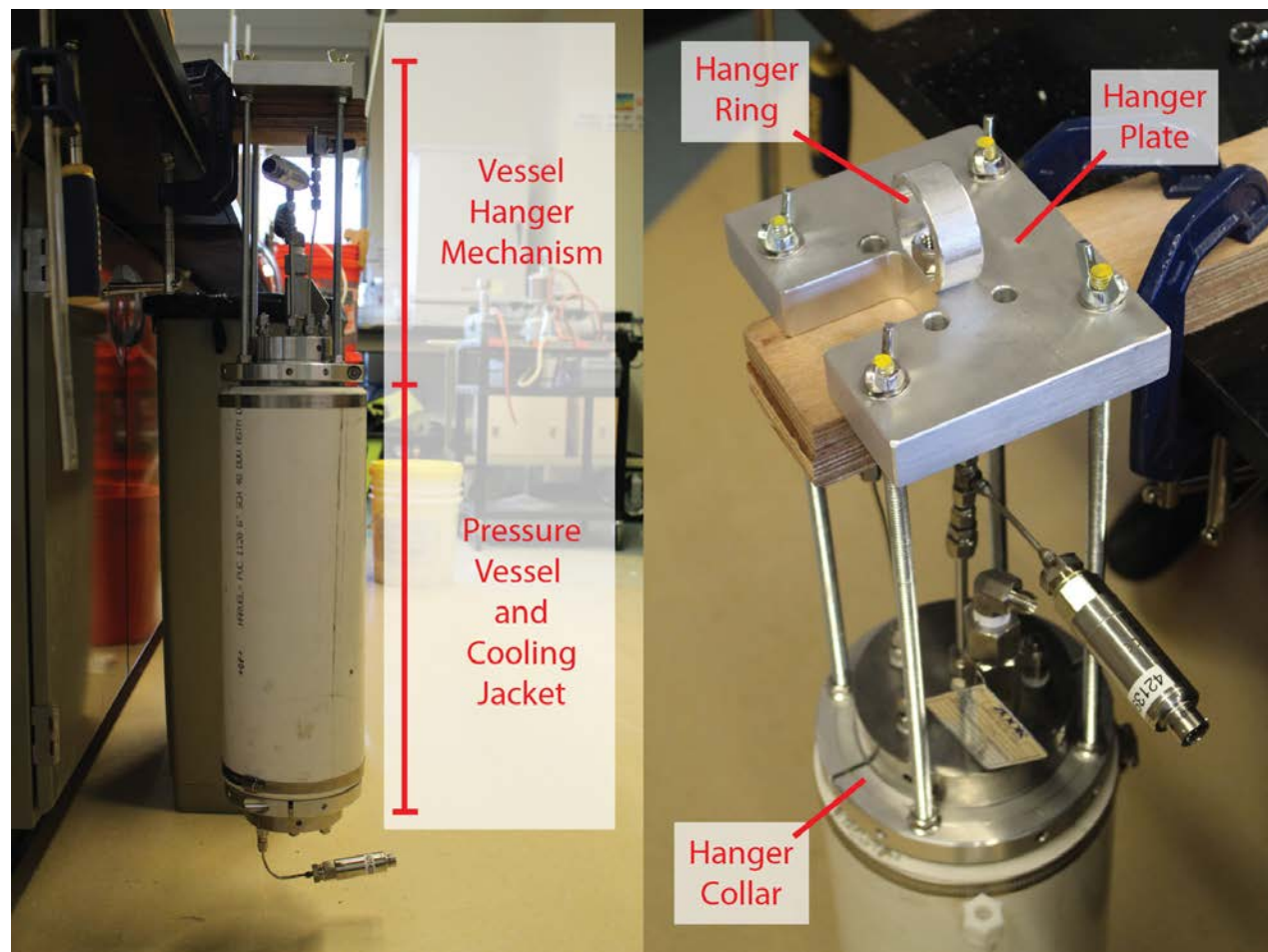

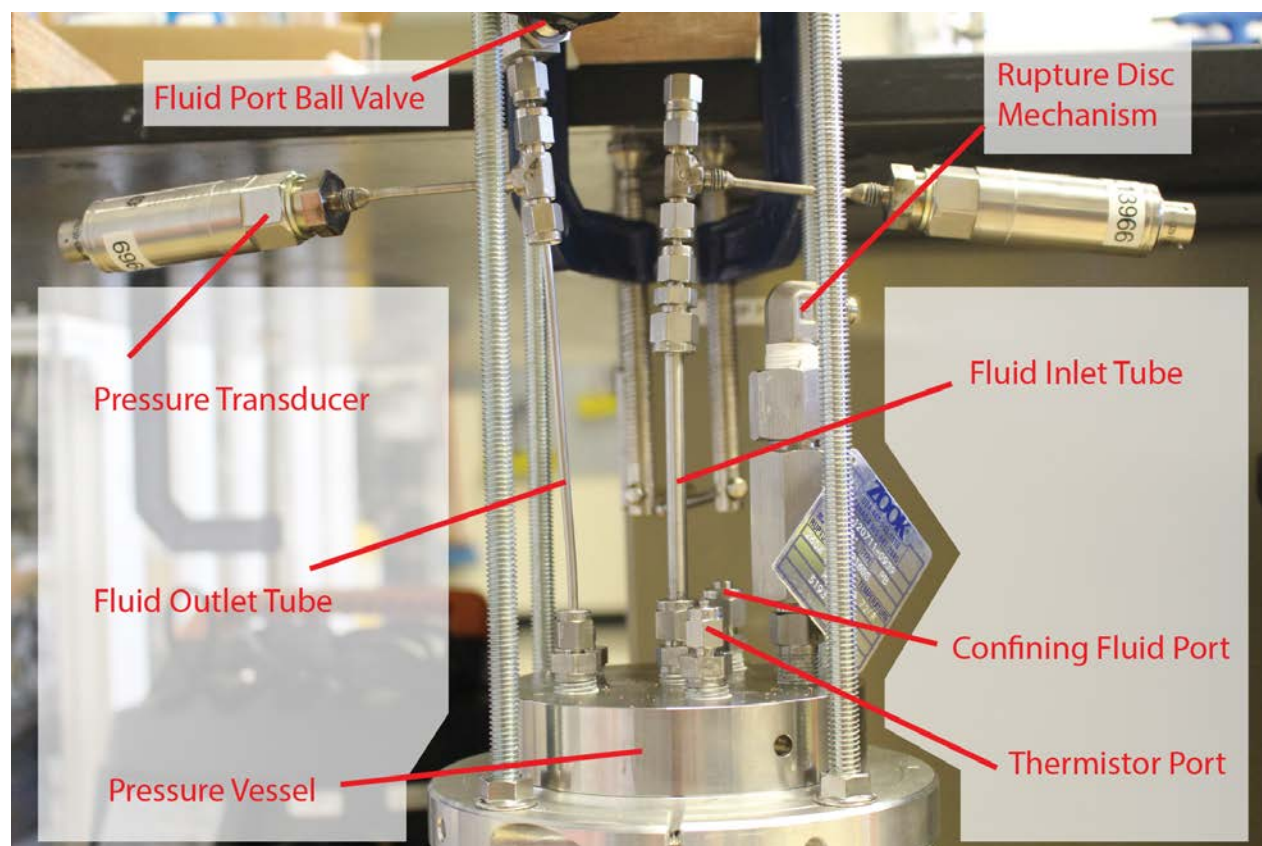**Figure 7: Pictures of large-scale vessel and hanger construction.**

Figure 8 Detailed view of the plumbing at the top of the vessel. The confining fluid plumbing, inlet port valve, and thermistor string are missing, but we have the materials necessary to build them.

Additionally, in preparation for the gas invasion experiments to be performed in the next quarter, we have designed an inline conductivity probe (Figure 9) that will allow us to determine when the gas phase has reached the outlet port of the sample as well as the salinity of the pore fluid. All the wires are potted with epoxy into a stainless steel tube and soldered to a 4-pin connector at the edge of the unit to prevent the wires from breaking and making the unit useless. Of the two outer wires one is grounded and the other is connected to standard alternating current, which will create an electrical field across the middle wires. The conductivity of the fluid is read between the two middle wires and is converted to resistivity using Ohm's Law. Eventually, when the fluid in the outlet tube changes from brine to gas, the resistivity read across the gold wires will go to infinity. This device is especially important to include in the experimental design for the dry runs, because we will not have CT scans to confirm when gas has reached the outlet port.
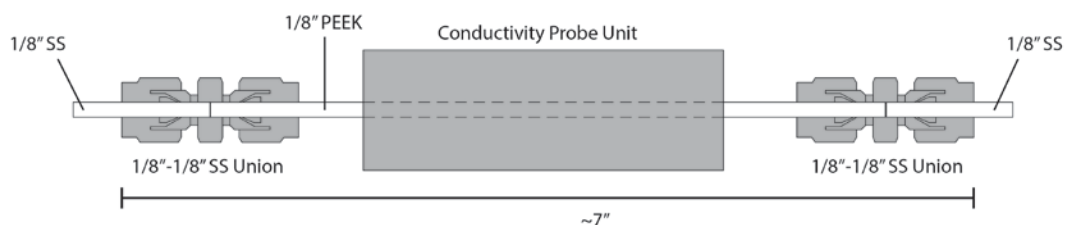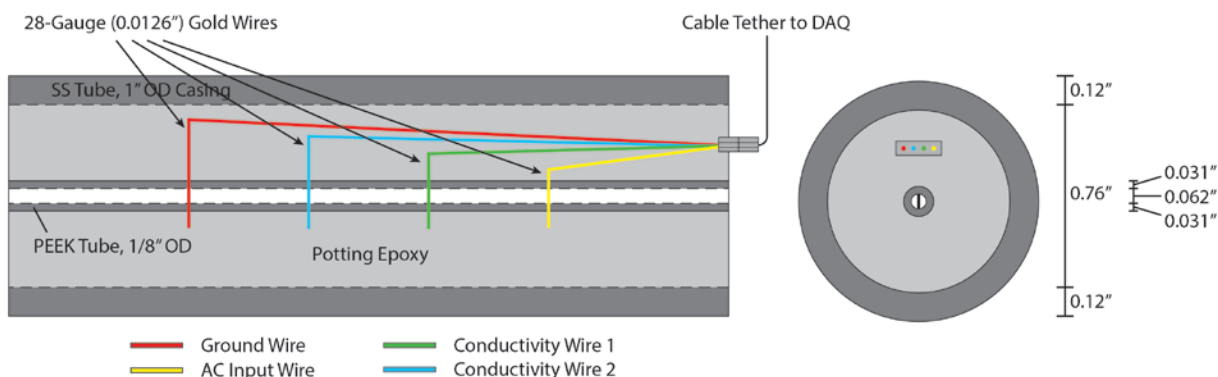
Conductivity Probe Inline Construction:

Conductivity Probe Unit Detail (2x zoom):

Figure 9: Schematic of the inline connectivity probe, which will be connected to the outlet port. It converts the stainless steel tube to non-conductive PEEK tubing, which is potted inside the conductivity probe unit. The probe consists of four gold wires that intersect the PEEK tubing at 0.5" spacing and lead to a 4-pin connector at one end of the unit. The wires and the connector are potted into a stainless steel tube using epoxy.

Subtask 6.2 - Gas invasion from melting hydrate into water saturated HSZ

Projected Finish: 9/28/15
Actual Finish: in process
We have not begun this task.

Task 7: 2D model

Projected Finish: 9/28/15
Actual Finish: in process

Subtask 7.1 - Hydrate dissociation in 2D systems

Projected Finish: 9/29/15
Actual Finish: in process
We have begun developing our 2D model.

Subtask 7.2 - Gas expulsion in 2D systems

Projected Finish: 3/30/15
Actual Finish: in process
We have begun to develop this model.

Subtask 7.3 - Apply 2D, gas expulsion model to natural examples

Projected Finish: 9/28/15
Actual Finish: pending
We have not begun this task.

Subtask 7.3.1 Pleistocene to Holocene Sea level rise

Projected Finish: 9/28/15
Actual Finish: pending
We have not begun this task.

Subtask 7.3.2 - Recent warming

Projected Finish: 9/28/15
Actual Finish: pending
We have not begun this task.

1.3 What opportunities for training and professional development has the project provided?

There has been strong interaction between UT and LBNL over this past quarter. Our graduate students and our post-doctoral scientist are now fully working with both institutions. A particularly ripe interface is that our students and post-doc are working closely with experimental efforts at LBNL. There is continuous interaction between petroleum engineering and geosciences as we address this problem.

1.4 How have the results been disseminated to communities of interest?

Paper Submissions
- Darnell, K.N., Flemings, P.B., and Bryant, S.L., in review, Transient venting of submarine arctic methane hydrate systems from moderate warming at seafloor, Geology.
- You, K., Kneafsey, T. J., Flemings, P. B., Polito, P., Bryant, S. L., accepted Jan 2015, Salinity-buffered methane hydrate formation and dissociation in gas-rich system, Journal of Geophysical Research: Solid Earth, doi:10.1002/2014JB011190

Abstract Submissions
- Darnell, K., Flemings, P.B., 2013, Methane hydrate destabilization sensitivity to physical complexity and initial conditions in a numerical model, Abstract presented at *2013 Fall Meeting*, AGU, San Francisco, Calif., 9-13 Dec.
- Kneafsey, T., Flemings, P.B., Bryant, S., You, K., Polito, P., 2013, Preliminary Experimental Examination Of Controls On Methane Expulsion During Melting Of Natural Gas Hydrate Systems, Abstract presented at *2013 Fall Meeting, AGU*, San Francisco, Calif., 9-13 Dec.
- Meyer, D., Flemings, P.B., 2013, Thermodynamic state of hydrate-bearing sediments on continental margins around the world, Abstract presented at *2013 Fall Meeting, AGU*, San Francisco, Calif., 9-13 Dec.
- Meyer, D., Flemings, P.B., 2014, Thermodynamic State of Hydrate-Bearing Sediments on Continental Margins around the World, Abstract presented at *2014 Offshore Technology Conference*, Houston, TX, 5-8 May.

- You, K., Flemings, P.B., Bryant, S., Kneafsey, T., Polito, P., 2014, Methane Hydrate Formation and Dissociation at Three-Phase Equilibrium at Constant Pressure, Abstract presented at *Gordon Research Conference: Natural Gas Hydrate Systems*, Galveston, TX, 23-28 March.

1.5 What do you plan to do during the next reporting period to accomplish the goals?

Task 5.00: Gas expulsion modeling
We will complete our write up of our 1D model to arctic systems. We will complete our write up of our analytical model describing gas expulsion and hydrate formation.

Task 6.00: Gas expulsion experiments
We will again work to simulate propagation of a gas front and hydrate formation at Berkeley. We will also build and test our hydrate cell that we have built at U.T.

Task 7.00: 2D model
We will begin continue work on this task.

2 PRODUCTS:

2.1 What has the project produced?

- We have now produced a one dimensional, coupled; hydrate formation code that simulates the thermo-chemical response of a hydrate system to perturbation.

- We have demonstrated three-phase stability through experimental analysis and we have modeled the behavior.

- We have also characterized the in-situ thermodynamic state of a number of hydrate locations around the world and shown that in at least two locations, local thermodynamic conditions are altered by high salinity.

- We have demonstrated an approach to estimate whether or not gas venting will occur for a given thermal perturbation.

- We have developed a model that couples both ice and hydrate solidification/melting in response to surface temperature change.

- We have developed an analytical model based on the method of characteristics to describe the propogation of gas into the hydrate stability zone.

- We have built a pressurized cell to simulate the formation of hydrate. .

3   PARTICIPANTS & OTHER COLLABORATING ORGANIZATIONS:

3.1   *What individuals have worked on the project?*

Provide the following information for: (1) principal investigator(s)/project director(s) (PIs/PDs); and (2) each person who has worked at least one person month per year on the project during the reporting period, regardless of the source of compensation (a person month equals approximately 160 hours of effort).

Name	Peter Flemings	Tim Kneafsey	Dylan Meyer	Kris Darnell	Kehua You
Project Role	Principal Investigator	Co-Principal Investigator	Graduate Student	Graduate Student	Post Doc
Nearest person month worked	.25	1.25	1	1	3
Contribution	Advised graduate students and post doc, and managed project. Worked with technicians for thermistor development.	Set up experiment, ran tests, and analyzed data.	Performed analysis of thermodynamic state of 4 locations.	Performed literature review and theoretical calculation to prepare for laboratory experiments	Performed literature review and theoretical calculation to prepare for laboratory experiments
Funding Support	The University of Texas	Lawrence Berkeley National Lab	JSG Fellowship	The University of Texas	The University of Texas
Collaborated with individual in foreign country	No	No	No	No	No

Name	Peter Polito	Tessa Green	David DiCarlo		
Project Role	Laboratory Manager	Project Coordinator	Advisor		
Nearest person month worked	1.5	1	.25		
Contribution	Participated in conference calls on experimental design. Ran experimental tests.	Coordinate meeting logistics, archive documents, and manage financials.	Advised students and worked with Peter Polito on lab related processes.		
Funding Support	The University of Texas	The University of Texas	The University of Texas		
Collaborated with individual in foreign country	No	No	No		

3.2   *What other organizations have been involved as partners?*

Organization Name: Lawrence Berkeley National Lab

Location of Organization: Berkeley, CA
Partner's contribution to the project (identify one or more)
- In-kind support: partner makes lab space and equipment available for experiments. (e.g., partner makes software, computers, equipment, etc., available to project staff);
- Facilities: Experiments are performed in partner's lab space using equipment largely supplied by the partner (e.g., project staff use the partner's facilities for project activities);
- Collaborative research: Partner collaborates with the project staff. (e.g., partner's staff work with project staff on the project); and

3.3   Have other collaborators or contacts been involved?

No

4   IMPACT:

4.1   What is the impact on the development of the principal discipline(s) of the project?

Geological models of gas transport and hydrate melting and solidification have suggested that free gas cannot migrate through the hydrate stability zone during melting. In contrast, we suggest that free gas can migrate through the hydrate stability zone by altering the conditions of hydrate stability to a state of three-phase equilibrium through the elevation of salinity and possibly temperature. This results in fundamentally different macro-scale behavior during melting and may result in greater gas venting than has been previously demonstrated. If this hypothesis is correct, it may engender a new generation of field and laboratory investigations to document this behavior in both the field of geosciences and petroleum engineering. Second, the project links theoretical development with laboratory modeling because the concepts can be applied at the laboratory scale as well as the field scale. The laboratory experiments to be conducted will enable validation of the mechanisms incorporated in the models. These laboratory experiments will play a key role in demonstrating the processes.

4.2   What is the impact on other disciplines?

A likely outcome of our work is a more quantitative prediction of the magnitude of methane flux from the earth to the atmosphere over human (decadal) timescales and geological timescales (10,000 years). These will serve as boundary conditions for atmospheric climate models. In turn, these results may guide policy decisions.

4.3   What is the impact on the development of human resources?

We are working at the interface of geosciences and engineering. We are coupling theory and laboratory experiments to address macro-scale geologic problems. This is training a new generation of geoscientists and engineers to think with a systems-based approach that links observation with theory.

The results are being applied in the classroom and the support is training several graduate students.

4.4   What is the impact on physical, institutional, and information resources that form infrastructure?

The project is strengthening the experimental efforts and capability at UT as it is our job to develop sensor equipment. The project is strengthening development at LBNL where primary experimental work is occurring.

4.5   What is the impact on technology transfer?

We are presenting our research to approximately 100 industry members at our GeoFluids consortium (Feb 2015) and we will be presenting at a range of national and international meetings.

4.6   What is the impact on society beyond science and technology?

A likely outcome of our work is a more quantitative prediction of the magnitude of methane flux from the earth to the atmosphere over human (decadal) timescales and geological timescales (10,000 years). These will serve as boundary conditions for atmospheric climate models. In turn, these results may guide policy decisions.

4.7   What dollar amount of the award's budget is being spent in foreign country(ies)?

Zero percent of the award's budget is being spent in foreign countries.

5   CHANGES/PROBLEMS:

5.1   Changes in approach and reasons for change

There are no changes in approach to report for this reporting period.

5.2   Actual or anticipated problems or delays and actions or plans to resolve them

Our biggest challenge is in the experimental realm. It has been more challenging than envisioned to simulate the solidification of hydrate with an advancing gas front. LBNL is also nearly spent out of resources. For this reason we have also built an experimental cell for application at U.T.

5.3   Changes that have a significant impact on expenditures

Dr. Steve Bryant moved to a new academic position effective Sept 1, 2014. As a result he was removed as Co-PI on this project. With approval from sponsor we reallocated unexpended salary plus indirect cost recovery to purchase permanent equipment

5.4   .Significant changes in use or care of human subjects, vertebrate animals, and/or Biohazards

Nothing to report

5.5   Change of primary performance site location from that originally proposed

Nothing to report

DOE Award No.: DE-FE0010406
DUNS No.: 170230239
Quarterly Research Performance Progress Report (Period ending 12/31/2014)
CONTROLS ON METHANE EXPULSION DURING MELTING OF NATURAL GAS HYDRATE SYSTEMS: TOPIC AREA 2

6 BUDGETARY INFORMATION:

Baseline Reporting (4/1/14 - 9/30/15)	Budget Period 2							
	Q1 4/1/2014-8/15/2014		Q2 8/16/2014-12/31/2014		Q3 1/1/2015-5/15/2015		Q4 5/16/2015-9/30/2015	
	Q1	Cumulative Total	Q2	Cumulative Total	Q3	Cumulative Total	Q4	Cumulative Total
Baseline Cost Plan								
Federal Share	$ 127,422.00	$ 788,535.00	$ 127,422.00	$ 915,957.00	$ 127,425.00	$ 1,043,382.00	$ 127,425.00	$ 1,170,807.00
Non-Federal Share	$ 34,048.50	$ 208,323.50	$ 34,048.50	$ 242,372.00	$ 34,048.50	$ 276,420.50	$ 34,048.50	$ 310,469.00
Total Planned	$ 161,470.50	$ 996,858.50	$ 161,470.50	$ 1,158,329.00	$ 161,473.50	$ 1,319,802.50	$ 161,473.50	$ 1,481,276.00
Actual Incurred Cost								
Federal Share	$ 202,625.00	$ 710,801.00	$ 117,194.00	$ 827,995.00	$ 28,278.00	$ 856,273.00	$ -	$ 856,273.00
Non-Federal Share	$ 27,408.75	$ 145,914.07	$ 27,408.75	$ 173,322.82	$ -	$ 173,322.82	$ -	$ 173,322.82
Total Incurred Cost	$ 230,033.75	$ 856,715.07	$ 144,602.75	$ 1,001,317.82	$ 28,278.00	$ 1,029,595.82	$ -	$ 1,029,595.82
Variance								
Federal Share	$ 75,203.00	$ (152,937.00)	$ (10,228.00)	$ (163,165.00)	$ (99,147.00)	$ (262,312.00)	$ (127,425.00)	$ (389,737.00)
Non-Federal Share	$ (6,639.75)	$ (55,769.67)	$ (6,639.75)	$ (62,409.43)	$ (34,048.50)	$ (96,457.93)	$ (34,048.50)	$ (130,506.43)
Total Variances	$ 68,563.25	$ (208,706.67)	$ (16,867.75)	$ (225,574.43)	$ (133,195.50)	$ (358,769.93)	$ (161,473.50)	$ (520,243.43)

7 Nomenclatures

Superscript

a downstream side of the leading shock

b upstream side of the leading shock

c downstream side of the trailing shock

d upstream side of the leading shock

e a position between the downstream side of the trailing shock and upstream side of leading shock

Subscript

B the component of brine

M the component of methane

W the component of pure water

g gas phase

h hydrate phase

l liquid water phase

β phase index

κ component index

cl_0 initial salinity (wt.%)

cl_e salinity at three phase equilibrium (wt.%)

D_s effective molecular diffusion coefficient of salt in sediment ($m^2 s^{-1}$)

D_{s0} molecular diffusion coefficient of salt in free water ($m^2 s^{-1}$)

f_g fractional flow of gas phase (dimensionless)

f_l fractional flow of liquid water phase (dimensionless)

g acceleration due to gravity ($m\ sec^{-2}$)

G_β overall dimensionless concentration of component β

H_β overall dimensionless flux of component β

k sediment intrinsic permeability (m^2)

k_0 sediment intrinsic permeability in absence of ice and hydrate (m^2)

$k_{r\beta}$ relative permeability of β phase (dimensionless)

L characteristic length (m)

L_s distance from the hydrate solidification front where salt diffusion changes the salinity (m)

P_c capillary pressure (Pa)

P_0 pressure (Pa)

q_{gi} gas injection rate ($m\ sec^{-1}$)

S_β^* effective saturation of β phase (dimensionless)

S_β saturation of β phase (dimensionless)

S_{gr}	residual gas phase saturation (dimensionless)
S_{wr}	residual water phase saturation (dimensionless)
t	time (sec)
T_0	temperature (^{o}C)
v	total flux of the mobile phase (m sec^{-1})
v_D	dimensionless total flux
$X_{\kappa,\beta}$	mass fraction of component κ in phase β (dimensionless)
θ	dip angle of the system (rad)
ϕ	porosity (dimensionless)
ρ_{lD}	dimensionless density of liquid water phase
ρ_{gD}	dimensionless density of gas phase
ρ_{hD}	dimensionless density of hydrate phase
ρ_{β}	density of β phase (kg m^{-3})
ρ_{gi}	density of the injected gas (kg m^{-3})
μ_{β}	dynamic viscosity of β phase (kg m^{-1} s^{-1})
λ_{β}	mobility of phase β (W m^{-1} ^{o}C^{-1})
τ	dimensionless time
ε	dimensionless distance from gas inlet
ε_0	initial dimensionless position of the composition G_{β}
Λ_{β}^{ab}	dimensionless leading shock velocity calculated by the component β
Λ^{e}	dimensionless composition wave velocity for gas saturation of S_g^e

8   References

Bader, S., and Kooi, H., 2005, Modelling of solute and water transport in semi-permeable clay
       membranes: comparison with experiments: Advances in Water Resources, v. 28, no. 3, p. 203-
       214.

Bangs, N. L. B., Hornbach, M. J., and Berndt, C., 2011, The mechanics of intermittent methane venting at
       South Hydrate Ridge inferred from 4D seismic surveying: Earth and Planetary Science Letters, v.
       310, no. 1, p. 8.

Barbour, S. L., and Fredlund, D. G., 1989, Mechanisms of osmotic flow and volume change in clay soils:
       Canadian Geotechnical Journal, v. 26, no. 4, p. 551-562.

Clennell, M. B., Hovland, M., Booth, J. S., Henry, P., and Winters, W. J., 1999, Formation of natural gas
       hydrates in marine sediments: 1. Conceptual model of gas hydrate growth conditioned by host
       sediment properties: Journal of Geophysical Research: Solid Earth, v. 104, no. B10, p. 22985-
       23003.

Daigle, H., Bangs, N. L., and Dugan, B., 2011, Transient hydraulic fracturing and gas release in methane hydrate settings: A case study from southern Hydrate Ridge: Geochemistry, Geophysics, Geosystems, v. 12, no. 12, p. 15.

Daigle, H., and Dugan, B., 2011, Capillary controls on methane hydrate distribution and fracturing in advective systems: Geochemistry, Geophysics, Geosystems, v. 12, no. 1, p. 18.

DiCarlo, D. A., Mirzaei, M., Aminzadeh, B., and Dehghanpour, H., 2012, Fractional Flow Approach to Saturation Overshoot: Transport in Porous Media, v. 91, no. 3, p. 955-971.

Ginsburg, G. D., and Soloviev, V. A., 1997, Methane migration within the submarine gas-hydrate stability zone under deep-water conditions: Marine Geology, v. 137, no. 1–2, p. 49-57.

Haacke, R. R., Hyndman, R. D., Park, K.-P., Yoo, D.-G., Stoian, I., and Schmidt, U., 2009, Migration and venting of deep gases into the ocean through hydrate-choked chimneys offshore Korea: Geology, v. 37, no. 6, p. 531-534.

Haeckel, M., Suess, E., Wallmann, K., and Rickert, D., 2004, Rising methane gas bubbles form massive hydrate layers at the seafloor: Geochimica et Cosmochimica Acta, v. 68, no. 21, p. 4335-4345.

Liu, and Flemings, P. B., 2007, Dynamic multiphase flow model of hydrate formation in marine sediments: Journal of Geophysical Research: Solid Earth, v. 112, no. B3, p. B03101.

Liu, X., and Flemings, P. B., 2006, Passing gas through the hydrate stability zone at southern Hydrate Ridge, offshore Oregon: Earth and Planetary Science Letters, no. 241, p. 16.

Malusis, M. A., Shackelford, C. D., and Olsen, H. W., 2003, Flow and transport through clay membrane barriers: Engineering Geology, v. 70, no. 3–4, p. 235-248.

Mazumdar, A., Dewangan, P., João, H. M., Peketi, A., Khosla, V. R., Kocherla, M., Badesab, F. K., Joshi, R. K., Roxanne, P., Ramamurty, P. B., Karisiddaiah, S. M., Patil, D. J., Dayal, A. M., Ramprasad, T., Hawkesworth, C. J., and Avanzinelli, R., 2009, Evidence of paleo–cold seep activity from the Bay of Bengal, offshore India: Geochemistry, Geophysics, Geosystems, v. 10, no. 6, p. Q06005.

Meyer, D. W., and Flemings, P. B., 2014, Thermodynamic State of Gas Hydrate in the Krishna-Godavari Basin Inferred From Well Log Analysis, Offshore Technology Conference 2014: Houston, TX, OnePetro.

Milkov, A. V., Dickens, G. R., Claypool, G. E., Lee, Y.-J., Borowski, W. S., Torres, M. E., Xu, W., Tomaru, H., Tréhu, A. M., and Schultheiss, P., 2004, Co-existence of gas hydrate, free gas, and brine within the regional gas hydrate stability zone at Hydrate Ridge (Oregon margin): evidence from prolonged degassing of a pressurized core: Earth and Planetary Science Letters, v. 222, no. 3–4, p. 829-843.

NGHP Expedition 01 Scientists, 2007, Sites NGHP-01-10, 12, and 13, *in* Collett, T. S., Reidel, M., Cochran, J., Boswell, R., Presley, J., Kumar, P., Sathe, A., Sethi, A., Lall, M., V., S., and the NGHP Expedition 01 Scientists, eds., National Gas Hydrate Program Expedition 01 Initial Reports, Directorate General of Hydrocarbon, Ministry of Petroleum and Natural Gas (India), p. 150.

Orr, F. M., 2007, Theory of Gas Injection Processes, Copenhagen, Denmark, Tie-Line Publications.

Rees, E. V. L., Priest, J. A., and Clayton, C. R. I., 2011, The structure of methane gas hydrate bearing sediments from the Krishna–Godavari Basin as seen from Micro-CT scanning: Marine and Petroleum Geology, v. 28, no. 7, p. 1283-1293.

Rehder, G., Brewer, P. W., Peltzer, E. T., and Friederich, G., 2002, Enhanced lifetime of methane bubble streams within the deep ocean: Geophysical Research Letters, v. 29, no. 15, p. 21-21-21-24.

Riedel, M., Collett, T. S., Kumar, P., Sathe, A. V., and Cook, A., 2010, Seismic imaging of a fractured gas hydrate system in the Krishna–Godavari Basin offshore India: Marine and Petroleum Geology, v. 27, no. 7, p. 1476-1493.

Ryu, B.-J., Collett, T. S., Riedel, M., Kim, G. Y., Chun, J.-H., Bahk, J.-J., Lee, J. Y., Kim, J.-H., and Yoo, D.-G., 2013, Scientific results of the Second Gas Hydrate Drilling Expedition in the Ulleung Basin (UBGH2): Marine and Petroleum Geology, v. 47, no. 0, p. 1-20.

Schneider, J., 2011, Compression and Permeability Behavior of Natural Mudstones [PhD Thesis: The University of Texas at Austin.

Torres, M. E., Kim, J. H., Choi, J. Y., Ryu, B. J., Bahk, J. J., Riedel, M., Collett, T. S., Hong, W. L., and Kastner, M., 2011, Occurrence of high salinity fluids associated with massive near-seafloor gas hydrate deposits, Proceedings of the 7th International Conference on Gas Hydrates: Edinburgh, Scotland, United Kingdom, p. 19.

Torres, M. E., Wallmann, K., Tréhu, A. M., Bohrmann, G., Borowski, W. S., and Tomaru, H., 2004, Gas hydrate growth, methane transport, and chloride enrichment at the southern summit of Hydrate Ridge, Cascadia margin off Oregon: Earth and Planetary Science Letters, v. 226, no. 1–2, p. 225-241.

Zatsepina, O. Y., and Buffett, B. A., 2003, Nucleation of gas hydrate in marine environments: Geophysical Research Letters, v. 30, no. 9, p. 1451.

National Energy Technology Laboratory

626 Cochrans Mill Road
P.O. Box 10940
Pittsburgh, PA 15236-0940

3610 Collins Ferry Road
P.O. Box 880
Morgantown, WV 26507-0880

13131 Dairy Ashford Road, Suite 225
Sugar Land, TX 77478

1450 Queen Avenue SW
Albany, OR 97321-2198

Arctic Energy Office
420 L Street, Suite 305
Anchorage, AK 99501

Visit the NETL website at:
www.netl.doe.gov

Customer Service Line:
1-800-553-7681